

## High harmonic generation without tunnel ionization

Jonathan Berkheim<sup>1</sup>, Eliyahu Bordo<sup>1</sup>, Eldar Ragonis<sup>1</sup>, Lev Merensky<sup>1</sup>, and Avner Fleischer<sup>1\*</sup>*Raymond and Beverly Sackler Faculty of Exact Sciences, School of Chemistry, Tel Aviv University, Tel Aviv 6997801, Israel and Tel-Aviv University center for Light-Matter-Interaction, Tel Aviv 6997801, Israel* (Received 3 January 2023; accepted 19 August 2023; published 9 November 2023)

A high harmonic generation (HHG) scheme, which does not rely on tunnel ionization as the ionization mechanism but rather on single-photon ionization, is theoretically proposed and numerically demonstrated. The scheme uses two driver fields: an extreme-ultraviolet driver which induces the ionization, and a circularly polarized, corotating, two-color infrared driver carried at a fundamental frequency and its second harmonic which induces the recollision. Using classical and time-dependent Schrödinger equation simulations of a model argon atom, we show that in this scheme ionization is essentially decoupled from recollision. Releasing the HHG mechanism from being tunneling dependent reduces its degree of nonlinearity, which offers interesting capabilities in attosecond science, such as generation of high harmonics from highly charged ions, or from specific deep core electronic levels. It is shown that the emitted high harmonics involve the absorption of photons of one color of the infrared driver, and the emission of photons of the second color. This calls for future examination of the possible correlations between the emitted high harmonics.

DOI: [10.1103/PhysRevResearch.5.043138](https://doi.org/10.1103/PhysRevResearch.5.043138)

### I. INTRODUCTION

High harmonic generation (HHG) is a central technique in attosecond science [1–3] and a prominent representative of extreme-nonlinear optical processes. In HHG intense infrared (IR) laser radiation is converted into the extreme ultraviolet (XUV) and soft x-ray regimes by interaction with gas, liquid [4–6], or solid medium [7–14]. Its strong nonlinearity stems from the event which initiates this three-step process [15]: tunnel ionization (tunneling) of a bound electron into the continuum. The two steps which follow are the propagation and recollision of the continuum electron with its remaining bound part, leading to the emission of short, attosecond bursts of radiation. This radiation source enables the tracking, exploration, and control of ultrafast electronic processes in atoms, molecules [16–19], and solids [20] in a tabletop lab setup.

The nonlinear features of tunneling, together with the inherent coupling between the ionization and recollision steps, impose fundamental and practical limitations in the HHG process. For instance, the maximal photon energy which can be achieved in the process, namely the cutoff energy  $\hbar\Omega_{\text{cutoff}}$  ( $\hbar$  is the Planck constant and  $\Omega_{\text{cutoff}}$  is the cutoff frequency), is limited to roughly 90 eV for argon driven by an 800-nm linearly polarized driver [21], irrespective of the driver intensity used. This results from the defocusing of the laser driver beam which accompanies excessive plasma generation. The plasma also adversely affects the coherent, phase-matched buildup of the HHG signal across the generation media [22]. Most

importantly, high levels of ionization and ground-state depletion reduce the photorecombination cross section already at the single emitter level. Since tunneling has extreme-nonlinear dependence on the IR driver's intensity, the restriction on the level of ionization limits the maximal effective driver intensity experienced by the media [23]. As the cutoff energy depends only linearly on the IR driver's intensity,  $\hbar\Omega_{\text{cutoff}} = I_p + 3.17U_p$  (where  $I_p$  is the ionization potential and  $U_p = \frac{q^2 E_{\text{IR}}^2}{4m\omega^2}$  is the ponderomotive energy, with  $q$ ,  $m$  being the electron's charge and mass, and  $E_{\text{IR}}$ ,  $\omega$  being the driver's amplitude and frequency, respectively) the cutoff energy becomes limited as well. The cutoff could be extended, albeit at the cost of considerable reduction in the HHG yield, if a driver with longer carrier wavelength is used [22,24] (the cutoff energy increases to about 300 eV in argon if the driver's wavelength is increased to 1600 nm). Increasing the ionization potential  $I_p$  of the media is another strategy (the cutoff energy increases to several keV if helium is driven at the same wavelength [21,22]). Given that the highest ionization potential of neutral species is only 24.6 eV (that of helium), the nonlinear dependence of tunneling on  $I_p$  imposes another limitation, as it excludes tunneling from deep-core electronic levels over tunneling from high-lying valence levels, or tunneling from cationic species [25] when a mixture of neutral and ionized media is used [26].

Replacement of the tunneling step in the HHG process with single-photon ionization (SPI), e.g., by absorption of a high-energy XUV photon of frequency  $\omega_{\text{XUV}}$ , could in principle remove the above-mentioned limitations. However when a linearly polarized IR driver is used the recollision is adversely affected [27] by the initial momentum

$$k_0 = \sqrt{\frac{2m(\hbar\omega_{\text{XUV}} - I_p)}{\hbar^2}} \quad (1)$$

\*Corresponding author: [avnerfleisch@tauex.tau.ac.il](mailto:avnerfleisch@tauex.tau.ac.il)

with which the photoelectron appears in the continuum according to the photoelectric effect. Hence, in previous studies the inclusion of XUV drivers has been mostly utilized for the excitation of Rydberg states from which tunneling by an IR field is easier [28–30], for the transfer of electrons to the continuum for streaking or photoionization studies [31–33 and references therein] or as a spectroscopic tool [34–35 and references therein]. Only mild improvement of the HHG yield or cutoff energy has been obtained [32,36–42]. In addition, in relativistic HHG the XUV photon can facilitate the recollision by providing an initial momentum which counteracts the drift imposed by the magnetic component of the relativistic IR driver [43].

Here we demonstrate a HHG scheme in which SPI replaces tunneling as the first step in the three-step model, while still providing an intense recollision. It consists of shining the generation media by a combination of a high-frequency XUV driver and an IR driver. The large frequency difference between the drivers ensures that the evolution of the electron occurs on two different time scales. Hence, by virtue of a Born-Oppenheimer-like separation of variables, the two drivers take separate roles: the high-frequency XUV field efficiently liberates the electron to the continuum by SPI (first step of the three-step model) but hardly affects the propagation in the continuum other than inducing a small quiver to the trajectory [44], while the IR driver is solely responsible for the propagation and recollision (second and third steps of the three-step model). In order to facilitate an intense recollision, the IR driver itself is a two-color, corotating circularly polarized field. We analyze this scheme using both classical trajectory analysis and time-dependent Schrödinger equation (TDSE) simulations and show that the phase, polarization direction, and frequency of the XUV driver determine the structure of the HHG spectra (HGS), while its intensity determines the HGS intensity.

## II. RESULTS AND DISCUSSION

### A. Classical treatment

In the context of HHG, a two-color circularly polarized, corotating IR driver field with carrier frequencies of fundamental  $\omega$  and its second harmonic ( $r = 2$ ),

$$\mathbf{E}_{\text{IR}}(t) = E_{\text{IR}} \left\{ \left[ -\cos\left(\omega t + \frac{\pi}{4}\right) - \cos\left(r\omega t + \frac{\pi}{4}\right) \right] \hat{x} + \left[ \sin\left(\omega t + \frac{\pi}{4}\right) + \sin\left(r\omega t + \frac{\pi}{4}\right) \right] \hat{y} \right\}, \quad (2)$$

is considered useless. For an electron initially at rest (as is the case when the electron is liberated by tunneling), this field does not manage to return the electron back to the origin. The absence of recollision is consistent with photon angular momentum (spin) conservation considerations. As each driver photon in the field of Eq. (2) already has a minimal spin of minus unity ( $\hbar = 1$ ), the parametric conversion of these photons into a high-energy photon is not possible [45,46]. The Lissajous curve of this field is given by the blue trace of Fig. 1(d) for  $\omega = 0.02848$  (wavelength of  $\lambda = 1600$  nm),  $r = 2$ , and  $E_{\text{IR}} = 0.03$  (intensity of  $I = 6.32 \times 10^{13}$  [W/cm<sup>2</sup>] for each color). We now show that this field could in fact generate efficient HHG provided that

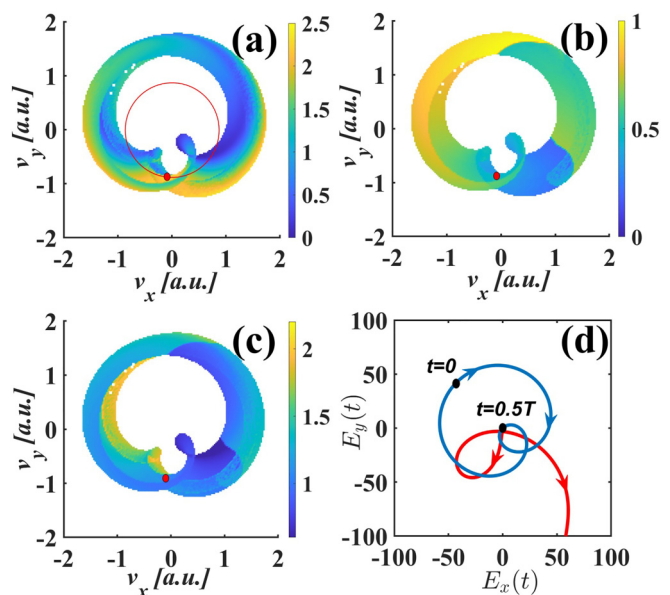


FIG. 1. (a) Averaged kinetic energy upon recollision  $\bar{E}_k(\mathbf{v})$  of all trajectories with initial velocity  $\mathbf{v} = [v_x, v_y]$  in units of the IR driver ponderomotive energy  $U_p$ . (b)  $\bar{t}_i(\mathbf{v})$  [T]. (c)  $\bar{t}_r(\mathbf{v})$  [T]. (d) Lissajous curve (scaled  $\times 1000$ ) of the field in Eq. (2) with  $r = 2$  (blue trace) and an exemplary cutoff trajectory (red trace). The red circle in (a) has a radius of 0.8839. Along this circle, the average kinetic energy is peaked for the initial velocity  $\mathbf{v} = [-0.125, 0.875]$  [marked by the red dots throughout Figs. 1(a)–1(c)].

an XUV field which liberates the electron to the continuum with a large initial velocity is added. We examine the classical trajectories resulting from the propagation of a free electron of charge  $q$  and mass  $m$  (atomic units are used throughout,  $m = -q = 1$ ), initially at the origin, freed at time  $t_i$  into the two-color IR field of Eq. (2). Integrating the classical Newton second-law equation twice, from the release time  $t_i$ , trajectories which return to the origin (termed “closed” or “recolliding” trajectories) at time  $t_r$  exist if the initial velocity (defined in column vector notation)  $\mathbf{v} \equiv [v_x, v_y]$  of the electron fulfills

$$0 = (t_r - t_i)\mathbf{v} + \frac{q}{m} \int_{t_i}^{t_r} dt' \int_{t_i}^{t'} dt'' \mathbf{E}_{\text{IR}}(t''). \quad (3)$$

For each value of the initial velocity  $\mathbf{v}$ , a group of several closed trajectories might exist, each having a unique release time and kinetic energy upon recollision  $E_{k,i}(\mathbf{v}) = \frac{1}{2m} [m\mathbf{v} + q \int_{t_i}^{t_r} dt' \mathbf{E}_{\text{IR}}(t')]^2$ . Figure 1(a) shows the average kinetic energy upon recollision,  $\bar{E}_k(\mathbf{v}) = \frac{\sum_i W_i E_{k,i}(\mathbf{v})}{\sum_i W_i}$ , of all trajectories having the initial velocity  $\mathbf{v}$ , in units of the Ponderomotive potential of the two-color IR field,  $U_p = \frac{q^2 E_{\text{IR}}^2}{2m\omega^2} (1 + \frac{1}{r^2})$ . The contribution of each trajectory is weighted according to its recombination cross section, which is assumed to inversely depend on the recolliding electronic wave-packet lateral spreading only, according to  $W_i = (t_r - t_i)^{-2}$ . Similarly, average values of the release times  $\bar{t}_i(\mathbf{v}) = \frac{\sum_i W_i t_i(\mathbf{v})}{\sum_i W_i}$  and recollision times  $\bar{t}_r(\mathbf{v}) = \frac{\sum_i W_i t_r(\mathbf{v})}{\sum_i W_i}$  are shown in units of the optical period  $T = \frac{2\pi}{\omega}$  in Figs. 1(b) and 1(c) respectively. It is

seen that the return of the electron to the origin is possible only if large values of initial velocities  $\mathbf{v}$  are given to the electron. In particular, when  $\mathbf{v} = \begin{bmatrix} -0.125 \\ -0.875 \end{bmatrix} \equiv \mathbf{v}^{\text{cutoff}}$  [red dots in Figs. 1(a)–1(c)] the cutoff trajectory and the maximal average kinetic energy upon recollision,  $\bar{E}_k(\mathbf{v}^{\text{cutoff}}) \approx 2.246U_p$ , are obtained, with release and recollision times being  $\bar{t}_i(\mathbf{v}^{\text{cutoff}}) = 0.469T$  and  $\bar{t}_r(\mathbf{v}^{\text{cutoff}}) = 1.077T$ . A specific cutoff trajectory representing this group of cutoff trajectories, with values  $\mathbf{v} = \begin{bmatrix} -0.125 \\ -0.875 \end{bmatrix}$ ,  $t_i = 0.469T$ ,  $t_r = 1.067T$ ,  $E_k(t_r = 1.067T) \approx 2.276U_p$ , is given by the red trace in Fig. 1(d). This trajectory starts at (returns to) the origin when the IR field's instantaneous amplitude is close to zero (maximal), in contrast to the cutoff trajectory in the traditional HHG scheme (based on tunnel ionization induced by a linearly-polarized monochromatic IR field).

### B. Quantum-mechanical treatment

SPI by high-frequency XUV driver field is capable of liberating electrons into the continuum with large initial velocity—a task which cannot be accomplished when the ionization is carried out by tunneling. Then, recollision could be induced by the field of Eq. (2). We demonstrate this by numerically solving the TDSE for a single electron in a 3D model of an argon atom in the length gauge,

$$\left[ -\frac{\hbar^2}{2m}\nabla^2 + V_0(r) - q\mathbf{r} \cdot \mathbf{E}(t) \right] \Psi(\mathbf{r}, t) = i\hbar \frac{\partial}{\partial t} \Psi(\mathbf{r}, t), \quad (4)$$

and the field-free potential is taken to be  $V_0(r) = \frac{-Z(r)}{\sqrt{r^2+a}}$  ( $r = \sqrt{\mathbf{r} \cdot \mathbf{r}}$ ) with  $Z(r) = 1 + 0.2719e^{-0.25r}$  and  $a = 0.09192$ , which yields the correct two lowest bound states of the argon atom [47]. The driver electric field is composed of two parts,  $\mathbf{E}(t) = f_{\text{IR}}(t)\mathbf{E}_{\text{IR}}(t) + f_{\text{XUV}}(t)\mathbf{E}_{\text{XUV}}(t)$ , where the XUV field,

$$\mathbf{E}_{\text{XUV}}(t) = E_{\text{XUV}}[-\cos(\omega_{\text{XUV}}t)\hat{x} + \sin(\omega_{\text{XUV}}t)\hat{y}], \quad (5)$$

is circularly polarized with the same helicity as the other two colors and  $E_{\text{XUV}}$  is its amplitude. Here both drivers' envelopes  $f_{\text{IR}}(t)$ ,  $f_{\text{XUV}}(t)$  are trapezoid with seven cycles of rising and falling edges and six cycles of plateau (in units of  $T$ ). We slightly detune ( $r = 1.95$ ) the second harmonic of the IR driver which causes the Lissajous curve to slowly drift (rotate) throughout the pulse. For times  $10T < t < 11T$  it acquires the trace given in the inset of Fig. 2. The XUV field amplitude is  $E_{\text{XUV}} = 0.01$  [ $I = 7.02 \times 10^{12}$  ( $\frac{\text{W}}{\text{cm}^2}$ )], and its carrier frequency is usually  $\omega_{\text{XUV}} = 34\omega$  unless otherwise stated. The HGSs were obtained by Fourier transforming the time dependent dipole acceleration expectation value  $\mathbf{a}(t) = \langle \Psi(\mathbf{r}, t) | -\nabla V_0 | \Psi(\mathbf{r}, t) \rangle + q\mathbf{E}(t)$ .

Figure 2 shows the TDSE simulation results. A reference spectrum where the system is driven by the two-color corotating IR field alone (no XUV field) is shown in the yellow curve. As expected, besides few low-order harmonics, no HHG is generated. The IR driver induces ionization by tunneling, with the ionization probability at the end of the pulse being  $P_{\text{ion}}(t = 20T) \approx 0.0327$ . Supplementing the IR driver field with the XUV driver changes the picture dramatically. Several traces are shown (see also Fig. 3 for more traces):  $\omega_{\text{XUV}} = 26\omega$  [green curve,  $P_{\text{ion}}(t = 20T) \approx 0.273$ ],  $\omega_{\text{XUV}} = 34\omega$  [red,  $P_{\text{ion}}(t = 20T) \approx 0.121$ ],  $\omega_{\text{XUV}} = 42\omega$  [blue,  $P_{\text{ion}}(t = 20T) \approx 0.071$ ], and  $\omega_{\text{XUV}} = 50\omega$  [cyan,

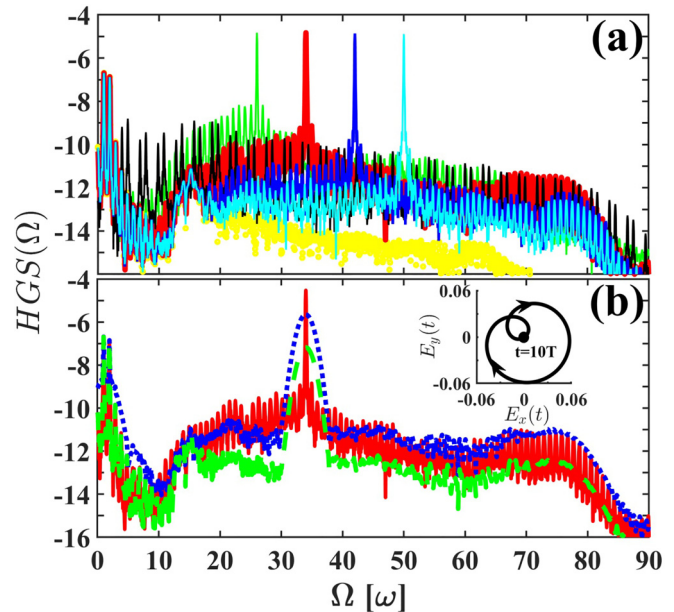


FIG. 2. (a) HGS (log scale) for the corotating ( $r = 1.95$ ) IR + XUV driver for  $\omega_{\text{XUV}} = 26\omega$  (green curve),  $\omega_{\text{XUV}} = 34\omega$  (red),  $\omega_{\text{XUV}} = 42\omega$  (blue), and  $\omega_{\text{XUV}} = 50\omega$  (cyan). Reference spectra where the system is driven by the corotating IR field only (no XUV field, yellow curve) and when the system is driven by a two-color, counter-rotating IR field only (no XUV field, black curve) are also shown. (b) HGS (log scale) for the corotating ( $r = 1.95$ ) trapezoid IR driver and short Gaussian pulse of circularly polarized XUV driver with  $\omega_{\text{XUV}} = 34\omega$  and  $E_{\text{XUV}} = 0.02108$  (dashed green curve), and a six-times-larger XUV amplitude (dotted blue curve). Red curve same as in (a). Inset: Lissajous curve (scaled  $\times 1000$ ) of the IR driver (black), which passes the origin at the arrival time of the XUV Gaussian pulse  $t_{\text{XUV}} = 10T$ . The Lissajous curve is rotated by  $\pi$  with respect to the one shown in Fig. 1(d) due to the drift imposed by the frequency ratio ( $r = 1.95$ ) of the IR driver constituents.

$P_{\text{ion}}(t = 20T) \approx 0.0513$ ]. In all cases intense HHG is obtained, comprised of discrete peaks, a plateau, and a cutoff. This seemingly contradiction to spin conservation (all driver photons are circularly polarized with same helicity) will be resolved later. Out of the traces shown, the HGS in the cutoff region ( $\Omega_{\text{cutoff}} \approx 75\omega$ ) is maximized for  $\omega_{\text{XUV}} = 34\omega$ . This is not surprising in light of the classical trajectory results presented in Fig. 1. With that XUV frequency, the cutoff recolliding trajectories are efficiently generated since the correct initial momentum is given to the electron by the XUV field:  $k_0 = \sqrt{\frac{2m(\omega_{\text{XUV}} - I_p)}{\hbar^2}} = \sqrt{\frac{2m(34\omega - I_p)}{\hbar^2}} = 0.8821$ , in accordance with the magnitude of the trajectory's initial velocity  $|\mathbf{v}^{\text{cutoff}}| = \sqrt{(-0.125)^2 + (-0.875)^2} = 0.8839$ . Also, with  $\bar{E}_k(\mathbf{v}^{\text{cutoff}}) \approx 2.246U_p \approx 54.7\omega$  and  $I_p \approx 0.579 \approx 20.34\omega$ , the group of cutoff trajectories are generating the cutoff HHG emission around  $\Omega_{\text{cutoff}} \approx 76\omega$ , as observed. For comparison, we show that the HGS of our scheme is comparable in intensity to the HGS obtained with the tunneling-based scheme of a two-color, counter-rotating IR driver [black curve,  $P_{\text{ion}}(t = 20T) \approx 0.0402$ ] [45,48–51].

In SPI, the ionization yield  $P_{\text{ion}}$  has linear dependence on the intensity of the XUV driver,  $P_{\text{ion}} \propto |E_{\text{XUV}}|^2$ ,

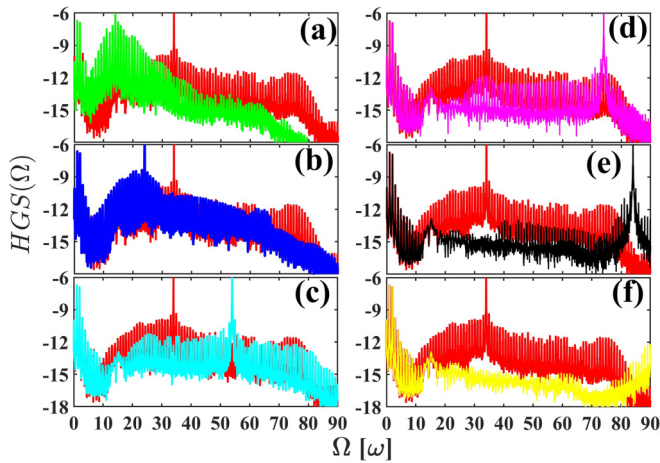


FIG. 3. (a) HGS (log scale) for the corotating ( $r = 1.95$ ) IR + XUV driver for  $\omega_{\text{XUV}} = 14\omega$  (green curve),  $\omega_{\text{XUV}} = 34\omega$  (red); (b)  $\omega_{\text{XUV}} = 24\omega$  (blue). (c)  $\omega_{\text{XUV}} = 54\omega$  (cyan). (d)  $\omega_{\text{XUV}} = 74\omega$  (magenta). (e)  $\omega_{\text{XUV}} = 84\omega$  (black). (f)  $\omega_{\text{XUV}} = 94\omega$  (yellow). Here longer driver pulses are taken:  $f_{\text{IR}}(t)$ ,  $f_{\text{XUV}}(t)$  are trapezoid with seven cycles of rising and falling edges, and 26 cycles of plateau (in units of  $T$ ). Due to the strong inverse dependence of SPI yield on the frequency of the XUV field, the XUV field amplitudes were taken as  $E_{\text{XUV}} = 0.00244, 0.00473, 0.00882, 0.0220, 0.0359, 0.0472, 0.0777$  (for the simulations in the green, blue, red, cyan, magenta, black and yellow curves respectively) such as to provide similar overall ionization yields in all traces:  $P_{\text{ion}}(t = 40T) \approx 0.120, 0.219, 0.209, 0.202, 0.177, 0.177, 0.212$ . As seen, the red curve ( $\omega_{\text{XUV}} = 34\omega$ ) provides the most intense HGS, with most extended cutoff.

and quadratic dependence,  $P_{\text{ion}} = \langle \psi_{\text{cont.}} | \psi_{\text{cont.}} \rangle$ , on the continuum part of the wave function  $\psi_{\text{cont.}}$ . Hence, the existence of recollision implies that the HGS intensity, which is related to the absolute-squared continuum-to-bound transition amplitude, should be linear in the XUV driver's intensity as well,  $\text{HGS}(\Omega) \sim |\langle \psi_b | -\nabla V | \psi_{\text{cont.}} \rangle|^2 \sim \sigma(|\psi_{\text{cont.}}|^2) \sim |E_{\text{XUV}}|^2$ . These two predictions are verified in Fig. 2(b) which shows the HGS simulated with all parameters as before ( $\omega_{\text{XUV}} = 34\omega$ ), but with the trapezoid XUV envelope replaced with a short Gaussian pulse,  $f_{\text{XUV}}(t) = \exp[-2 \ln 2 (\frac{t-t_{\text{XUV}}}{\tau_{\text{XUV}}})^2]$ , whose duration is  $\tau_{\text{XUV}} = 0.25T$ . In order to generate the cutoff trajectories, the short XUV pulse arrives at time  $t_{\text{XUV}} = 10T$ , when the IR field ( $r = 1.95$ ) crosses the origin. This time is very close to the release time  $\bar{t}_i(\mathbf{v}^{\text{cutoff}}) = 9.969T$  predicted by the classical trajectory calculations. The green curve shows the results with the XUV pulse with amplitude  $E_{\text{XUV}} = 0.02108$  [ $P_{\text{ion}}(t = 20T) \approx 0.03798$ ] and the blue curve shows the results where the XUV amplitude has been increased sixfold to  $E_{\text{XUV}} = 0.1265$  [ $P_{\text{ion}}(t = 20T) \approx 0.2055$ ]. Subtracting the tunneling-induced ionization [ $P_{\text{ion}}(t = 20T) \approx 0.0327$ ] from the total ionization probabilities gives the contribution of the XUV ionization event alone; a ratio of  $(0.2055 - 0.0327)/(0.03798 - 0.0327) \sim 32.7$  is obtained, in good agreement with the predicted ratio of 36. The two HGS traces also show a 36-fold increase in the HGS in the spectral region of the plateau and cutoff, as anticipated. Moreover, the continuous shape of the HGS (rather than a comblike structure) with the short-pulse

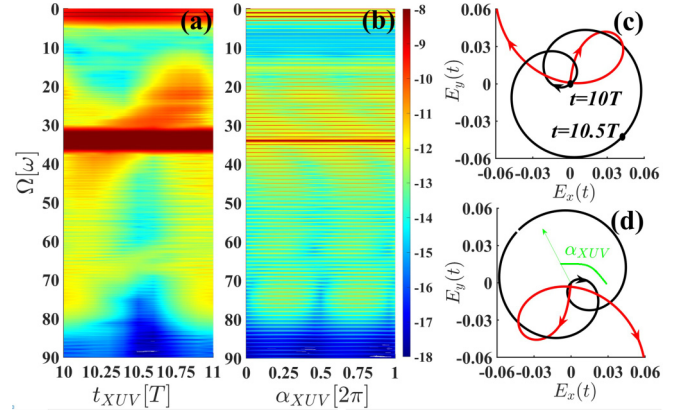


FIG. 4. (a) HGS (log scale) for the corotating trapezoid IR driver ( $r = 1.95$ ) and short Gaussian pulse of circularly polarized XUV driver with  $\omega_{\text{XUV}} = 34\omega$  for various arrival times  $t_{\text{XUV}}$  of the XUV driver field. (b) HGS for the corotating trapezoid IR driver ( $r = 2$ ) and linearly polarized XUV driver for various polarization directions of the XUV driver field. (c) Lissajous curve of the IR driver (black) and cutoff trajectory with  $\mathbf{v} = \begin{bmatrix} 0.125 \\ 0.875 \end{bmatrix}$  (red) corresponding to the simulations of panel (a) with  $t_{\text{XUV}} = 10T$ . (d) Lissajous curve of the IR driver (black) and cutoff trajectory with  $\mathbf{v} = \begin{bmatrix} -0.125 \\ -0.875 \end{bmatrix}$  (red) corresponding to the simulations of (b) with XUV pulses polarized along the  $y$  direction ( $\alpha_{\text{XUV}} = \pm \frac{\pi}{2}$ ).

XUV ionizer is another indication that recollision occurs in the process. As the electron is born during a single short time window, only a single recollision event occurs. These results prove that our proposed HHG scheme indeed involves recollision and SPI-initiated ionization, and that they are separated.

As our scheme suggests, a temporal synchronization between the XUV ionization and the IR driver is critical in order to ensure the recollision. This was indeed verified [Fig. 4(a)] by analyzing the dependence of the HGS on  $t_{\text{XUV}}$ . As anticipated, the HGS in the cutoff region is maximized for  $t_{\text{XUV}} \approx 10T$  since then the Lissajous curve of the two-color IR field crosses the origin [Fig. 4(c)] Moreover, a directional synchronization is needed as well. This is demonstrated by fixing in space the Lissajous curve for the IR driver ( $r = 2$ ) and taking a linearly polarized XUV field whose polarization direction creates an angle  $\alpha_{\text{XUV}}$  with the  $x$  axis. Our initial state has a  $1s$  spherical symmetry, which results in a Malus-type sin-square dependence of the HGS yield (in the plateau and cutoff) on  $\alpha_{\text{XUV}}$  [Fig. 4(b)]. This is in accordance with the anticipated linear dependence of the HGS on the flux of XUV-generated photoelectrons, the trajectory picture, and the  $p$ -shaped ionization distribution of electrons in the continuum typical of SPI from a state with  $s$  symmetry. The maximal HGS yield is obtained when the XUV polarization direction coincides with the  $y$  axis, since this leads to the birth of recollision trajectories [Fig. 4(d)]. On the other hand, if the XUV polarization direction coincides with the  $x$  axis, photoelectrons are released in all directions but the  $y$  direction, leading to a great suppression of the HGS.

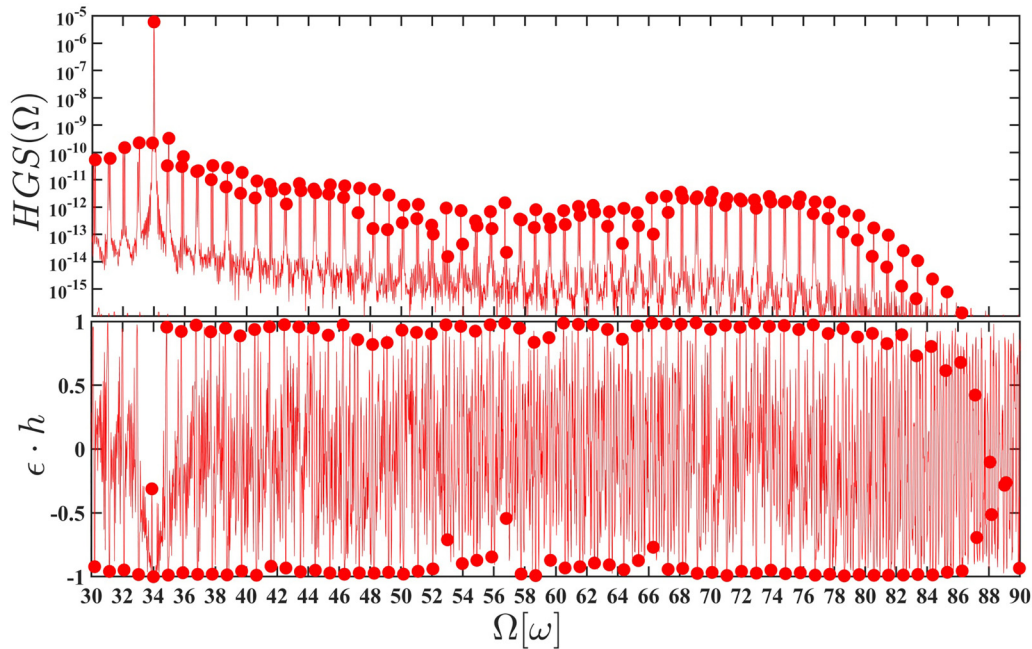


FIG. 5. (a) HGS for the corotating ( $r = 1.95$ ) IR + XUV driver  $\omega_{\text{XUV}} = 34\omega$  and long trapezoid pulses. (b) Ellipticity-helicity of the obtained harmonics.

### C. Photonic-picture considerations

Finally, we relate the semiclassical description described above to the photonic-picture description of HHG and photonic conservation laws. In the simulations presented above [excluding those of Fig. 4(b)] the spins of all three colors of driver photons have been deliberately chosen as minus unity,  $\sigma_1 = \sigma_2 = \sigma_{\text{XUV}} = -1$ . In such driver configuration spin conservation excludes the absorption of driver photons and emission of a *single* high-energy photon, since it is not possible for a photon spin to exceed unity. Since nevertheless intense HHG is observed, this means that more than a single photon is emitted in the HHG process. Figure 5 shows the HGS and ellipticity-helicity product of a simulation with  $r = 1.95$ ,  $\omega_{\text{XUV}} = 34\omega$  and longer trapezoid driver pulses [trapezoid envelopes with seven cycles of rising and falling edges, and 36 cycles of plateau (in units of  $T$ )]. The narrow harmonic peaks obtained enable the unique identification of harmonic emission channels according to their energy and polarization state. As it has been unequivocally identified that the HHG process is linear in the intensity of the XUV driver, only a single XUV driver photon is annihilated. All in all, four families of emission channels have been identified, all yielding circularly polarized photons. The first family are emission channels of the form  $\Omega_{(-n,n,1)}$  (where the integer numbers in the parentheses refer to the number of annihilated photons from each color,  $\omega_1$ ,  $\omega_2$ ,  $\omega_{\text{XUV}}$ , of the drivers, respectively, and a negative integer describes an emission of driver photons back to the driver field). This channel has an energy  $\Omega_{(-n,n,1)} = (-n)\omega_1 + n\omega_2 + 1\omega_{\text{XUV}} = n(\omega_2 - \omega_1) + \omega_{\text{XUV}}$  and spin  $\sigma_{(-n,n,1)} = (-n)(-1) + n(-1) + 1(-1) = -1$ . A specific channel which belongs to the first family is for instance  $\Omega_{(-20,20,1)} = 53\omega$ ,  $\sigma_{(-20,20,1)} = -1$ . In this channel, 20 photons of the second IR driver and a single photon of the XUV driver are absorbed (a total of 21 photons) and 21

photons are emitted: 20 photons back to the first color driver, and a single high-energy photon. The re-emission of driver photons removes excess spin from the system and enables this emission channel. A representative of the second family is, e.g.,  $\Omega_{(-24,22,1)} = 52.9\omega$ ,  $\sigma_{(-24,22,1)} = +1$ . In the other two families photons are emitted back to the second IR color, e.g.,  $\Omega_{(20,-20,1)} = 15\omega$ ,  $\sigma_{(20,-20,1)} = -1$  and  $\Omega_{(16,-18,1)} = 14.9\omega$ ,  $\sigma_{(16,-18,1)} = +1$ . In all channels IR photons of one color are annihilated and IR photons of the second color are emitted. This fact, in particular in light of the structure of the emission channels  $\Omega_{(-n,n,1)}$  and  $\Omega_{(n,-n,1)}$ , suggests that the high-harmonic photons might be correlated. This should be checked in future studies.

### III. CONCLUSION

To summarize, we have presented an HHG scheme in which the electron is liberated into the continuum by SPI rather than by tunneling. The recollision is induced by a well-synchronized two-color, circularly polarized, corotating IR field with correct frequencies and amplitudes to return the electron to the ion despite the initial velocity it acquired from the XUV ionizing field. Our scheme has several unique properties: First, the ionization step is separated from the propagation/recollision steps. The ionization is performed by the XUV field, while the propagation and recombination are controlled by the IR field. This means that the shape of the HGS could be controlled separately from the HHG efficiency: the IR field controls the shape and cutoff of the spectrum (by virtue of the recollisions and attochirp curve), while the spectrum's intensity depends linearly on the intensity of the XUV driver. Second, the ionization by SPI allows the generation of high harmonics from electronic levels which are hardly accessible when tunneling is concerned, e.g., those of

charged ions, or specific deep core electronic levels. Third, in order to generate recolliding trajectories, the XUV frequency and the IR frequency and intensity must be related according to Eqs. (1) and (3). In addition, the temporal synchronization and relative polarization directions between the XUV and IR drivers determine which trajectories participate in the recollision. Fourth, implementing our scheme in free-electron-laser facilities offers a possible route to efficiently convert the long pulses of bright XUV radiation routinely generated at these facilities to a train of short attosecond pulses or even an isolated attosecond pulse (by incorporating a short two-color,

circularly polarized, corotating driver which would induce a single recollision).

The presented HHG mechanism relies on the emission of several photons and not just a single one. It is reasonable to assume that some or all of the emitted harmonics are probably correlated.

#### ACKNOWLEDGMENT

This work was supported by the Israel Science Foundation (Grant No. 524/19).

- 
- [1] P. Corkum and F. Krausz, Attosecond science, *Nat. Phys.* **3**, 381 (2007).
- [2] F. Krausz and M. Ivanov, Attosecond physics, *Rev. Mod. Phys.* **81**, 163 (2009).
- [3] M. Nisoli, P. Decleva, F. Calegari, A. Palacios, and F. Martin, Attosecond electron dynamics in molecules, *Chem. Rev.* **117**, 10760 (2017).
- [4] A. D. DiChiara, E. Sistrunk, T. A. Miller, P. Agostini, and Louis F. DiMauro, An investigation of harmonic generation in liquid media with a mid-infrared laser, *Opt. Exp.* **17**, 20959 (2009).
- [5] T. T. Luu, Z. Yin, A. Jain, T. Gaumnitz, Y. Pertot, J. Ma, and H. J. Wörner, Extreme-ultraviolet high-harmonic generation in liquids, *Nat. Commun.* **9**, 3723 (2018).
- [6] O. Neufeld, Z. Nourbakhsh, N. Tancogne-Dejean, and A. Rubio, *Ab initio* cluster approach for high harmonic generation in liquids, *J. Chem. Theory Comput.* **18**, 4117 (2022).
- [7] S. Ghimire, A. D. DiChiara, E. Sistrunk, P. Agostini, L. F. DiMauro, and D. A. Reis, Observation of high-order harmonic generation in a bulk crystal, *Nat. Phys.* **7**, 138 (2011).
- [8] G. Vampa, T. J. Hammond, N. Thire, B. E. Schmidt, F. Legare, C. R. McDonald, T. Brabec, and P. B. Corkum, Linking high harmonics from gases and solids, *Nature (London)* **522**, 462 (2015).
- [9] T. T. Luu, M. Garg, S. Yu. Kruchinin, A. Moulet, M. Th. Hassan, and E. Goulielmakis, Extreme ultraviolet high-harmonic spectroscopy of solids, *Nature (London)* **521**, 498 (2015).
- [10] Y. S. You, D. A. Reis, and S. Ghimire, Anisotropic high-harmonic generation in bulk crystals, *Nat. Phys.* **13**, 345 (2017).
- [11] K. F. Lee, X. Ding, T. J. Hammond, M. E. Fermann, G. Vampa, and P. B. Corkum, Harmonic generation in solids with direct fiber laser pumping, *Opt. Lett.* **42**, 1113 (2017).
- [12] G. Vampa, Y. S. You, H. Liu, S. Ghimire, and D. A. Reis, Observation of backward high-harmonic emission from solids, *Opt. Express* **26**, 12210 (2018).
- [13] S. Ghimire and D. A. Reis, High-harmonic generation from solids, *Nat. Phys.* **15**, 10 (2019).
- [14] T. Heinrich, M. Taucer, O. Kfir, P. B. Corkum, A. Staudte, C. Ropers, and M. Sivi, Chiral high-harmonic generation and spectroscopy on solid surfaces using polarization-tailored strong fields, *Nat. Commun.* **12**, 3723 (2021).
- [15] P. B. Corkum, Plasma perspective on strong field multiphoton ionization, *Phys. Rev. Lett.* **71**, 1994 (1993).
- [16] S. Baker, J. Robinson, C. Haworth, H. Teng, R. A. Smith, C. C. Chirilă, M. Lein, J. W. G. Tisch, and J. P. Marangos, Probing proton dynamics in molecules on an attosecond time scale, *Science* **312**, 424 (2006).
- [17] O. Smirnova, Y. Mairesse, S. Patchkovskii, N. Dudovich, D. Villeneuve, P. Corkum, and M. Y. Ivanov, High harmonic interferometry of multi-electron dynamics in molecules, *Nature (London)* **460**, 972 (2009).
- [18] S. Haessler, J. Caillat, W. Boutu, C. Giovanetti-Teixeira, T. Ruchon, T. Auguste, Z. Diveki, P. Breger, A. Maquet, B. Carré, R. Taïeb, and P. Salières, Attosecond imaging of molecular electronic wavepackets, *Nat. Phys.* **6**, 200 (2010).
- [19] F. Lépine, G. Sansone, and M. J. Vrakking, Molecular applications of attosecond laser pulses, *Chem. Phys. Lett.* **578**, 1 (2013).
- [20] A. L. Cavalieri, N. Müller, T. Uphues, V. S. Yakovlev, A. Baltuška, B. Horvath, B. Schmidt, L. Blümel, R. Holzwarth, S. Hendel, M. Drescher, U. Kleineberg, P. M. Echenique, R. Kienberger, F. Krausz, and U. Heinzmann, Attosecond spectroscopy in condensed matter, *Nature (London)* **449**, 1029 (2007).
- [21] B. Shan and Z. Chang, Dramatic extension of the high-order harmonic cutoff by using a long-wavelength driving field, *Phys. Rev. A* **65**, 011804(R) (2001).
- [22] T. Popmintchev, M.-C. Chen, D. Popmintchev, P. Arpin, S. Brown, S. Ališauskas, G. Andriukaitis, T. Balčiūnas, O. D. Mücke, A. Pugzlys, A. Baltuška, B. Shim, S. E. Schrauth, A. Gaeta, C. Hernández-García, L. Plaja, A. Becker, A. Jaron-Becker, M. M. Murnane, and H. C. Kapteyn, Bright coherent ultrahigh harmonics in the keV x-ray regime from mid-infrared femtosecond lasers, *Science* **336**, 1287 (2012).
- [23] D. M. Rayner, A. Naumov, and P. B. Corkum, Ultrashort pulse non-linear optical absorption in transparent media, *Opt. Express* **13**, 3208 (2005).
- [24] J. Tate, T. Auguste, H. G. Muller, P. Salières, P. Agostini, and L. F. DiMauro, Scaling of wave-packet dynamics in an intense midinfrared field, *Phys. Rev. Lett.* **98**, 013901 (2007).
- [25] E. A. Gibson, A. Paul, N. Wagner, R. Tobey, S. Backus, I. P. Christov, M. M. Murnane, and H. C. Kapteyn, High-order harmonic generation up to 250 eV from highly ionized argon, *Phys. Rev. Lett.* **92**, 033001 (2004).
- [26] D. Popmintchev *et al.*, Ultraviolet surprise efficient soft x-ray high-harmonic generation in multiply ionized plasmas, *Science* **350**, 1225 (2015).
- [27] K. J. Schafer, M. B. Gaarde, A. Heinrich, J. Biegert, and U. Keller, Strong field quantum path control using attosecond pulse trains, *Phys. Rev. Lett.* **92**, 023003 (2004).

- [28] P. Johnsson, J. Mauritsson, T. Remetter, A. L'Huillier, and K. J. Schafer, Attosecond control of ionization by wave-packet interference, *Phys. Rev. Lett.* **99**, 233001 (2007).
- [29] D. D. A. Clarke, H. W. van der Hart, and A. C. Brown, Extreme-ultraviolet-initiated high-order harmonic generation in Ar<sup>+</sup>, *Phys. Rev. A* **97**, 023413 (2018).
- [30] A. C. Brown and H. W. van der Hart, Extreme-ultraviolet-initiated high-order harmonic generation: Driving inner-valence electrons using below-threshold-energy extreme-ultraviolet light, *Phys. Rev. Lett.* **117**, 093201 (2016).
- [31] J. Mauritsson, P. Johnsson, E. Mansten, M. Swoboda, T. Ruchon, A. L'Huillier, and K. J. Schafer, Coherent electron scattering captured by an attosecond quantum stroboscope, *Phys. Rev. Lett.* **100**, 073003 (2008).
- [32] K. L. Ishikawa, Efficient photoemission and ionization of He<sup>+</sup> by a combined fundamental laser and high-order harmonic pulse, *Phys. Rev. A* **70**, 013412 (2004).
- [33] C. Figueira de Morisson Faria, P. Salières, P. Villain, and M. Lewenstein, Controlling high-order harmonic generation and above-threshold ionization with an attosecond-pulse train, *Phys. Rev. A* **74**, 053416 (2006).
- [34] M. Krüger, D. Azoury, B. D. Brunner, and N. Dudovich, The role of electron trajectories in XUV-initiated high-harmonic generation, *MDPI Appl. Sci.* **9**, 378 (2019).
- [35] J. Leeuwenburgh, B. Cooper, V. Averbukh, J. P. Marangos, and M. Ivanov, High-order harmonic generation spectroscopy of correlation-driven electron hole dynamics, *Phys. Rev. Lett.* **111**, 123002 (2013).
- [36] J. Biegert, A. Heinrich, C. P. Hauri, W. Kornelis, P. Schlup, M. P. Anscombe, M. B. Gaarde, K. J. Schafer, and U. Keller, Control of high-order harmonic emission using attosecond pulse trains, *J. Mod. Opt.* **53**, 87 (2006).
- [37] A. Heinrich, W. Kornelis, M. P. Anscombe, C. P. Hauri, P. Schlup, J. Biegert, and U. Keller, Enhanced VUV-assisted high harmonic generation, *J. Phys. B* **39**, S275 (2006).
- [38] E. J. Takahashi, T. Kanai, K. L. Ishikawa, Y. Nabekawa, and K. Midorikawa, Dramatic enhancement of high-order harmonic generation, *Phys. Rev. Lett.* **99**, 053904 (2007).
- [39] G. Gademann, F. Kelkensberg, W. K. Siu, P. Johnsson, M. B. Gaarde, K. J. Schafer, and M. J. J. Vrakking, Attosecond control of electron-ion recollision in high harmonic generation, *New. J. Phys.* **13**, 033002 (2011).
- [40] D. Azoury, M. Krüger, G. Orenstein, H. R. Larsson, S. Bauch, B. D. Brunner, and N. Dudovich, Self-probing spectroscopy of XUV photo-ionization dynamics in atoms subjected to a strong-field environment, *Nat. Commun.* **8**, 1453 (2017).
- [41] A. D. Bandrauk and N. H. Shon, Attosecond control of ionization and high-order harmonic generation in molecules, *Phys. Rev. A* **66**, 031401(R) (2002).
- [42] A. D. Bandrauk, S. Chelkowski, and S. Goudreau, Control of harmonic generation using two-colour femtosecond-attosecond laser fields: Quantum and classical perspectives, *J. Mod. Opt.* **52**, 411 (2005).
- [43] M. Klaiber, K. Z. Hatsagortsyan, C. Muller, and C. H. Keitel, Coherent hard x-rays from attosecond pulse train-assisted harmonic generation, *Opt. Lett.* **33**, 411 (2008).
- [44] A. Fleischer, Generation of higher-order harmonics upon the addition of high-frequency XUV radiation to IR radiation: Generalization of the three-step model, *Phys. Rev. A* **78**, 053413 (2008).
- [45] A. Fleischer, O. Kfir, T. Diskin, P. Sidorenko, and O. Cohen, Spin angular momentum and tunable polarization in high-harmonic generation, *Nat. Photon.* **8**, 543 (2014).
- [46] E. Pisanty, S. Sukiasyan, and M. Ivanov, Spin conservation in high-order-harmonic generation using bicircular fields, *Phys. Rev. A* **90**, 043829 (2014).
- [47] A. Fleischer, P. Sidorenko, and O. Cohen, Generation of high-order harmonics with controllable elliptical polarization, *Opt. Lett.* **38**, 223 (2013).
- [48] H. Eichmann, A. Egbert, S. Nolte, C. Momma, B. Wellegehausen, W. Becker, S. Long, and J. K. McIver, Polarization-dependent high-order two-color mixing, *Phys. Rev. A* **51**, R3414(R) (1995).
- [49] S. Long, W. Becker, and J. K. McIver, Model calculations of polarization-dependent two-color high-harmonic generation, *Phys. Rev. A* **52**, 2262 (1995).
- [50] O. Kfir *et al.*, Generation of bright phase-matched circularly-polarized extreme ultraviolet high harmonics, *Nat. Photon.* **9**, 99 (2015).
- [51] Á. Jiménez-Galán, N. Zhavoronkov, D. Ayuso, F. Morales, S. Patchkovskii, M. Schloz, E. Pisanty, O. Smirnova, and M. Ivanov, Control of attosecond light polarization in two-color bicircular fields, *Phys. Rev. A* **97**, 023409 (2018).